

Review

Design of Hydroxyapatite-Based Multifunctional Nanoparticles for Cell Labelling and Cell Growth Inhibition

Takuya Kataoka¹, Kota Shiba^{2,3,4}, Motohiro Tagaya^{1,*}

¹ Department of Materials Science and Technology, Nagaoka University of Technology, Kamitomioka 1603-1, Nagaoka, Niigata 940-2188, Japan

² Center for Functional Sensor & Actuator (CFSN), National Institute for Materials Science (NIMS), 1-1 Namiki, Tsukuba, Ibaraki 305-0044, Japan

³ World Premier International Research Center Initiative (WPI), International Center for Materials Nanoarchitectonics (MANA), National Institute for Materials Science (NIMS), 1-1 Namiki, Tsukuba, Ibaraki 305-0044, Japan

⁴ John A. Paulson School of Engineering and Applied Sciences (SEAS), Harvard University, 9 Oxford Street, Cambridge, Massachusetts 02138, USA

* Correspondence: Motohiro Tagaya, Email: tagaya@mst.nagaokaut.ac.jp; Tel.: +81-258-47-9345.

ABSTRACT

There has been an increasing demand for the development of cell-labeling nanomaterials that safely label and visualize a specific type of cells for diagnosis and inspection in vivo and in vitro. In order to design such cell-labeling nanomaterials, the properties of efficient visible light luminescence and effective interactions with cells have to be realized using a biocompatible nanomaterial. From this viewpoint, we summarize and overview the current situation on cell-labeling technologies. Among various functional nanomaterials, we focus on hydroxyapatite nanoparticles and their photofunctionalization based on the properly designed inorganic-organic hybrid structure such as hydroxyapatite/organic europium (III) complex. Also, the immobilization technique of a specific binding molecule to the solid surface is introduced to demonstrate the selective uptake into cancer cells. Moreover, an example of the growth inhibitory drug molecules for cancer cells are described, focusing on the cytostatic inhibition of citric acid and the potential use of hydroxyapatite/citric acid hybrids. Finally, we mention our future perspectives on the theranostic nanoparticles with fluorescence and therapeutic properties that are achieved through the hydroxyapatite-organic hybrid interfacial interactions.

Open Access

Received: 29 August 2019

Accepted: 04 December 2019

Published: 09 December 2019

Copyright © 2019 by the author(s). Licensee Hapres, London, United Kingdom. This is an open access article distributed under the terms and conditions of [Creative Commons Attribution 4.0 International License](https://creativecommons.org/licenses/by/4.0/).

KEYWORDS: inorganic-organic nanohybrid systems; photofunctional interface; bio-imaging nanoparticles; cancer cell imaging; cancer cell therapy; hydroxyapatite nanoparticles; europium (III) complex; citric acid

INTRODUCTION

Pathological diagnosis and noninvasive therapy have been extensively investigated so far by means of a variety of techniques. Among them, nanomaterials that can bind to the surface of cells and fluoresce by light irradiation with a specific wavelength are well-known as cell-labeling nanomaterials and have been widely utilized for various purposes [1–4]. Many different types of cell-labeling technologies have been developed for the diagnosis of cancer cells including radioisotopes for single photon emission computed tomography (SPECT), positron emission tomography (PET) [5], iron-nanoparticles for magnetic resonance imaging (MRI) [6], and antibody-mediated labeling with optical probes [7]. However, the application of these techniques to early-stage cancer cells is still a grand challenge in this field. In order to overcome various difficulties, one of the keys would be to develop diagnostic techniques using a fluorescence endoscope to detect the epithelial cancer cells.

Other important features that are demanded for the cell-labeling nanomaterials are that they can safely label and visualize the cancer cells for diagnosis and inspection *in vivo* and *in vitro*. To realize such cell-labeling nanomaterials, nanomaterial itself has to be biocompatible, efficiently fluoresce in the visible light range (400–800 nm) as well as effectively interact with the cells. For the early stage detection of the cancer cells *in vivo*, the surface layer of the cells is stained to be observed with a fluorescence endoscope. Then, the cells are diagnosed on the basis of autofluorescence which is known as a fluorescence emitted by cell constituents. A previous study reported that clear luminescence peaks were observed at approximately 500 nm and 630 nm when excited at a wavelength of 437 nm [8]. However, the luminescence intensity of autofluorescence is too weak to confirm with our naked eyes, limiting practical use of this phenomenon to various applications. For this reason, many researchers have started from *in vitro* studies to achieve luminescence that can sufficiently be observed with a fluorescent endoscope, probably leading to the cell diagnosis *in vivo* afterwards. Although the detection limit of a confocal laser scanning microscope in *z* direction is known to be approx. 500 nm [9], some holographic microscopes can observe almost 30 μ m in depth from the cellular top surface. Taking advantage of these techniques, the cell-labeling nanomaterials can be utilized for immunoassay to diagnose early stage cancer in the visible light region.

To further develop and optimize nanomaterials with desired cell labeling properties, a possible mechanism on how the nanomaterials are captured by cells is considered in relation to the basic structure of cells. Endocytosis is known as one of the representative processes in which the nanomaterial is taken into the cell from the outside via the cell membrane [10]. There are two types of endocytosis: phagocytosis and pinocytosis. Phagocytosis is a mechanism that cells take up foreign substances (bacteria, viruses, parasites) and abnormal metabolites into the cell (tissue,

blood, etc.) and decompose them. Phagocytosis occurs only in a specific type of cells such as phagocytic cells, monocytes, dendritic cells, NK cells and neutrophils. Pathogens, dead cells and cell debris (1 μm or more) are also included. On the other hand, pinocytosis refers to the phenomenon that cells take up nanomaterials as vesicles regardless of their permeability. Internalization of substances with the size less than 300 nm [11] and 50 to 80 nm [12] into cells have been reported. No clear consensus has been obtained so far with respect to the mechanism of nanomaterial uptake into cells. The surface physical properties are regarded as one of the important factors, while the uptake behavior also varies depending on the types of cells. Since proteins and nanomaterials in vivo bind to each other and agglutinate, the cellular uptake mechanism does not depend only on the size of the nanomaterials. Pinocytosis depends on the size, composition and structure of the nanomaterial surface.

In this review, we summarize and overview some aspects and future challenges of the cell-labeling techniques. The cell-labeling techniques have the potential to be improved by the development of cytocompatible photoluminescence probes [13,14]. For example, lanthanide (Ln) ion-doped nanomaterials provide several advantages such as lower cytotoxicity, photostability and sharp luminescence bands over the conventional cell-labeling nanomaterials including organic molecules and semiconductor quantum dots [15,16]. From this viewpoint, we describe the importance of photofunctionalization of hydroxyapatite, which is realized by designing the inorganic-organic nanohybrid structures. We also highlight the surface immobilization technique of nanomaterials, making it possible to control uptake into cancer cells.

CELL-LABELING NANOMATERIALS

Labeling Mechanism

Figure 1 shows an outline of the labeling mechanism (endocytosis). On the basis of the interaction between a nanomaterial surface and cell membrane (receptor), endocytosis is classified into two behaviors: passive and active. The former is a weak liquid phase interaction such as hydrogen bonding, a hydrophobic effect and van der Waals force. In such cases, the nanomaterials are easily taken into the cells since surface energy is same as that of cell surfaces. The latter is a strong liquid phase/solid phase interaction such as ionic bonding, metal bonding and covalent bonding, etc. In the case of the strong interaction, the catalytic effect at the interaction point inhibits cellular uptake because of the high surface tension. The nanomaterial taken up by the cell is carried to the lysosome, then hydrolyzed and digested by enzymes. Likewise, the cell-labeling nanomaterial is taken into the cell through the interaction with the receptor present on the surface of the cell membrane, and fluorescence is emitted by the excitation of visible light. The luminescence emitted from cells in vitro can be detected with a fluorescence microscope and used for

diagnosis. Similarly, in vivo, it is detected with a fluorescence endoscope and used for diagnosis under the visible light excitation.

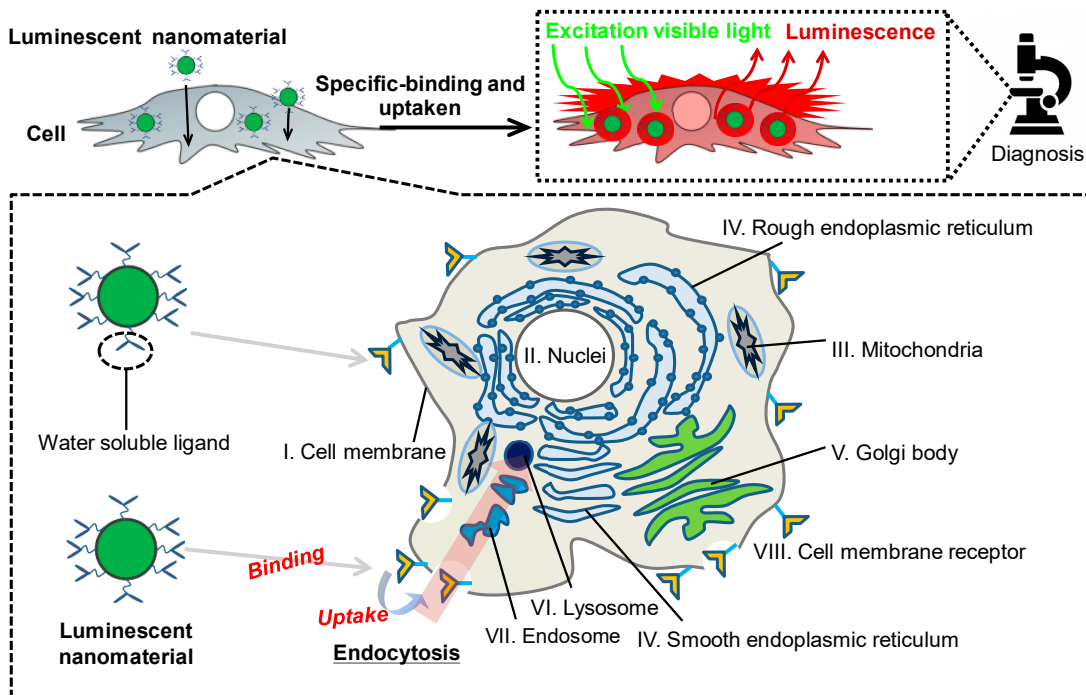


Figure 1. Illustration of the possible cell-labeling mechanism for diagnosis. The site to be taken into the cell is different depending on the particle size as described in the text.

Conventional Nanomaterials

Organic molecules

Organic molecules and inorganic nanoparticles have been used as cell-labeling nanomaterials. Depending on the nanomaterial, there are some problems such as fast color degradation which is due to ultraviolet light excitation, damaging the living tissue (influence of active oxygen generated by photochemical reaction, damage of biomolecules due to electron transfer reaction, etc.). A variety of nanomaterials have been synthesized so far; however, there are still no suitable nanomaterials to solve such problems. Some examples of cell-labeling nanomaterials already reported and known problems are shown in **Table 1**. For the organic molecules, a fluorescent protein (excitation wavelength: 400 nm) [17], fluorescent organic small molecule (excitation wavelength: 370 nm) [18], temperature responsive polymers (excitation wavelength: 456 nm) [19] and pH responsive dye (excitation wavelength: 532 nm) [20] have been reported. Such cell-labeling nanomaterials are not cytotoxic and do not affect cell function and cell growth behavior. Fluorescent proteins are less toxic to living bodies and emit luminescence through the visible light excitation. However, the protein can be decomposed by the light irradiation, affecting the function of cell-labeling. In the case of fluorescent organic low molecules, their fluorescence properties are affected by the molecular size which frequently causes steric hindrance. Although no

such drawbacks are seen with the temperature responsive and pH responsive dyes, some other difficulties including water insolubility and aggregate formation limit their usage in cell-labeling applications. For this kind of applications, it is necessary to synthesize nanomaterials which have sufficient stability in their color and luminescence properties even under continuous/strong light excitation.

Table 1. Conventional cell-labeling nanomaterials of organic molecular state solved in solution and inorganic particle state dispersed in solution, and their problems [13,14,16,17,19–23].

	Luminescent nanomaterial	Problem	Reference
Organic molecular state solved in solution	Fluorescent proteins	Decomposition and denaturation of protein by excitation light irradiation	[17]
	Temperature-responsive polymers	Aqueous insolubility by an easy aggregation	[19,20]
	pH-responsive dyes		
Inorganic particle state dispersed in solution	Semiconductor quantum dots	Containing biotoxic elements such as Cd and Hg	[13,14,21]
	Lanthanide (Ln) ion-doped oxides	Low quantum efficiency	[16,22,23]

Inorganic nanoparticles

Among various inorganic nanoparticles, semiconductor quantum dots (excitation wavelength: 260 nm) have been mainly utilized for cell-labeling applications [21] because of their strong luminescence and stable color. However, a problem has been also reported in terms of biotoxicity which is induced by compositional Cd, Hg, etc. (biotoxic element) [13,14,21]. These heavy metals are known to affect the cell function and reduce cell viability, possibly leading to undesirable and/or unexpected results in in vivo experiments. In addition, since the quantum dots are usually excited by UV light irradiation, potential damage to the cells is also concerned. To solve this problem, a Ln ion-doped oxide which is excited by the light with longer wavelength has been reported as the cell-labeling nanomaterial [16,22,23], while its luminescent properties and safety to cells are unknown yet (**Table 1**).

In order to overcome these barriers, a Ln ion-doped hydroxyapatite (HA) would be one of the model nanomaterials. HA has an excellent affinity with cells so that it can be used as a cell label. It is possible to synthesize cell-labeling HA-based nanomaterials with an excellent cell affinity by doping Ln ions that have low toxicity to living bodies and are capable of being excited by a low energy light in the visible range. Needless to say, the luminescent species (Ln ions) have to be incorporated into HA structure in such a way that their amount, spatial distribution and so on are controlled.

APPLICATION OF HYDROXYAPATITE FOR CELL-LABELING NANOMATERIALS

Hydroxyapatite

Features

The HA ($\text{Ca}_{10}(\text{PO}_4)_6(\text{OH})_2$) with a Ca/P ratio of 1.67 is an inorganic component contained in living tissues (bones and teeth), the crystal system is hexagonal, the space group is P63/m, and the unit cell is $0.94 \text{ nm} \times 0.94 \text{ nm} \times 0.68 \text{ nm}$ [24]. As a crystal structure, the four columnar Ca (i.e., Ca (I) site) is aligned parallel to the *c* axis, and the six screw axis Ca (i.e., Ca (II) site) surround the *c*-axis. Also, hydroxyl groups are present in the part surrounded by the screw Ca. The crystal structure of HA is shown in **Figure 2**. The high biocompatibility due to having a composition close to the hard tissues *in vivo* is an advantage, and applied study as a biomaterial is proceeding. The reported particle size of HA is around 20–300 nm [25,26], and it has excellent light resistance. The uptake of the HA nanoparticles with a size of 50–200 nm by the osteoblasts has been investigated, exhibiting the excellent uptake efficiency without cytotoxicity [27]. The Ca ions in the HA can be easily substituted with the other metal ions, and by substituting Ln ions, a luminescence property can be imparted. By using the HA matrix, it is possible to achieve the cell-labeling nanomaterials that are safe for the living body and do not affect the color degradation and luminescence properties due to the light excitation. Furthermore, since it is possible to impart the other functions (e.g., drug delivery carrier) for achieving the multi-functional particles, it is important to design the cell-labeling nanomaterials as nanoparticle shapes.

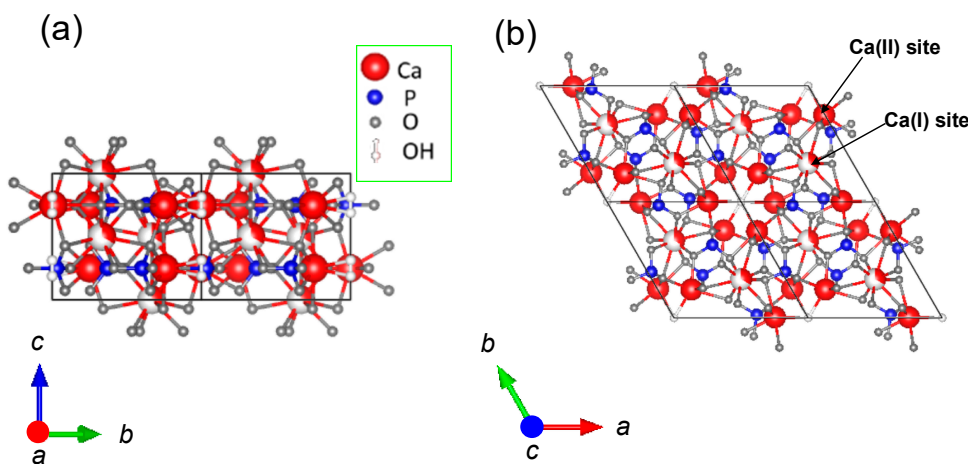


Figure 2. Crystalline structures of HA viewed from the (a) *a*- and (b) *c*-axis directions.

Hybrid systems with organic molecules *in vivo*

Figure 3 shows examples of inorganic-organic hybrids. **Figure 3a,b** shows the hierarchical structure of the chiton. The chiton is known to concentrate as much as 100,000 ppm of iron in teeth. In general, although

organisms often use calcium as the main component when forming hard tissues such as teeth, there are few organisms that form teeth with magnetite (Fe_2O_3) as the main component. The hydroxyl group of lepidochroite (α -, γ - FeOOH) is exposed on the surface, and exists as an inorganic-organic hybrid by interacting with α -chitin and proteins [28–30]. This inorganic-organic hybrid is achieved by the chemical bond of the Fe^{2+} ion of α - and γ - FeOOH with the carboxyl group and hydroxyl group in the α -chitin and proteins.

The bone tissue *in vivo* is also the same. **Figure 3c,d** is a schematic diagram of bone tissue *in vivo*. HA is the main component of bone *in vivo*, and it forms a chemical bond at the interface with collagen and exists as the inorganic-organic hybrid. This hybrid was achieved by the chemical bonding of Ca ions in HA and carboxyl groups in collagen fibril on the interface. The action of organisms to form minerals is called biomineralization and it is known to also occur *in vivo*.

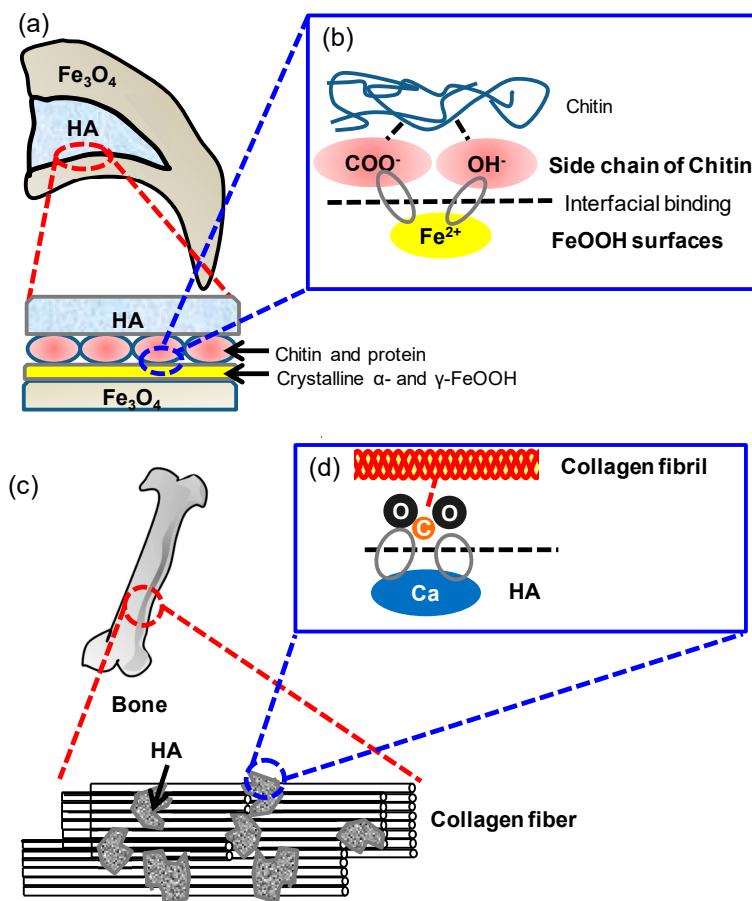


Figure 3. (a, c) Hierarchical structures of inorganic-organic hybrids at (a, b) teeth of chiton and (c, d) cancellous bone tissue, and their (b, d) interfacial interactions in the binding state at the molecular level.

The study on the synthesis of functional nanoparticles has been conducted using biomineralization [31,32]. The possibility of the development of the novel cell-labeling nanoparticles by mimicking biomineralization is expected.

Incorporation of Hydroxyapatite Nanoparticles into Cells

The interaction between cytophilic nanoparticles and cells depends on the particle size, surface structure, chemical composition, solubility and aggregation. These are important for circulation in the body, invasiveness to lesions and accumulation, and can be expected to improve the effects of diagnosis and therapy.

The substances diffuse into the cells due to the concentration gradient. The transport of the substances inside and outside the cell membranes by the concentration gradient without chemical change is called as passive transport [33]. In the passive transport, the substance is transported by the concentration gradient. On the other hand, transporting the substances against the concentration gradient is called as active transport [34]. The active transport is performed by a pump in the cell using the hydrolysis energy of adenosine triphosphate. However, the selective intracellular targeting is difficult to be done using these intracellular transports. Therefore, we have been focusing on the transport through endocytosis, and the selective cellular uptake can be achieved by designing the surface immobilization states of the nanoparticles. Since several endocytosis-mediated cellular uptake mechanisms have been proposed, the size of the nanoparticle to be incorporated is also an important factor in cellular uptake. As previously mentioned, the uptake of HA nanoparticles with a size of 50–200 nm (100 µg/mL) has been reported in osteoblasts [35]. In particular, the particle size of about 80 nm for HA particles has been reported to be good for cellular uptake. Specifically, the cells taking up the HA nanoparticles showed the same growth behavior as non-incorporated cells, and the cell affinity with the particles alone was confirmed. It has already been defined that there is toxicity to cells when the cell growth rate is less than 130% in 6 h of culture [36]. As an international standards, the nanoparticle is defined as non-cytotoxicity, if the decrease rate in the cell viability during the cell culture is 30% or less as compared with the case in the cells without the nanoparticle [37]. The HA particles can be judged to be non-cytotoxic in the size range of 50–200 nm [35] according to previous reports [36,37]. For the cell-labeling, the particle sizes of HA in a media bound to the cells via endocytosis was approximately 120 nm [38]. Thus, HA is suitable as the matrix for the cell-labeling nanoparticles.

Possibility of Imaging by Photofunctionalization

Hybrids with functional low molecular compounds such as 8-hydroxyquinoline (8Hq) [39,40] and glucosamine [41] on a nanoscale have already been reported. For example, in the HA/8Hq system, the 8Hq molecules were chemically bonded to the Ca²⁺ ions on the HA by applying mechanical forces. The photofunction of the hybrids has been studied by evaluating the light absorption and luminescence through the metal-ligand charge transfer complex formation. In the HA/glucosamine system, glucosamine molecules were hybridized with HA due to the hydrogen-

bonding interactions between the amino and hydroxyl groups of glucosamine and the hydroxyl groups on the surface of HA. No study has been done yet to hybridize a photofunctional dye (visible light responsive) and HA and use them as cell labels. Several studies of the europium (III) ion (Eu^{3+}) doped HA have been reported [42,43]. For example, when the Eu^{3+} doped HA was synthesized in the presence of cetyltrimethylammonium bromide as a cationic surfactant, the substitution efficiency of the Eu^{3+} ion into the Ca (II) site of HA was enhanced [44]. However, the low quantum yield is a problem when compared to existing the cell-labeling nanoparticles.

Thus, detailed understanding of the photophysicochemical driving force at the interface with organic molecules on the HA surface is considered to be important for the design of novel cell-labeling nanoparticles.

Europium (III) ION

Photochemical Properties

For the Ln ions, most of the absorption and luminescence transitions in the infrared to near-ultraviolet region are due to transitions between the split $4f$ orbital levels [45,46]. The electric dipole transition between energy levels belonging to the same electron configuration becomes a forbidden transition by the selection rule of evenness and oddity. However, when atoms or ions are in a solid or in a liquid, the $5d$ level on the $4f$ level mixes with the $4f$ level due to the effect of the crystal field, resulting in an allowable transition. Even in the case of the crystal field having an inversion symmetry, it is permitted to some extent by coupling with the lattice vibration having odd properties. The transition probability changes depending on the symmetry of the ligand field and the electronic state of the Ln ion. The $4f$ orbitals of the Ln ions are shielded by the $5s$ and $5p$ orbitals [47], which increases the fluorescence lifetime. The six electrons in the $4f$ shell can be arranged into seven $4f$ orbitals. The degeneracy of a $4f_n$ electronic configuration is given by the binomial coefficient using the following Equation (1).

$$\binom{14}{n} = \frac{14!}{n!(14-n)!} \quad (1)$$

where n is the number of $4f$ electrons. The n of Eu^{3+} is 6. The energy diagram of the Eu^{3+} ion is shown in **Figure 4**. All the peaks corresponded to the transitions from the metastable orbital singlet state of $^5\text{D}_0$ to the spin-orbital states of $^7\text{F}_J$ ($J = 0, 1, 2, 3, 4$) of the Eu^{3+} ion. J represents the total angular momentum. These characteristic transitions were assigned to the $^5\text{D}_0$ to $^7\text{F}_0$ at about 575 nm, $^7\text{F}_1$ at about 590 nm, $^7\text{F}_2$ at about 616 nm, $^7\text{F}_3$ at about 653 nm and $^7\text{F}_4$ at about 698 nm, respectively. In particular, the transitions of $^5\text{D}_0$ to $^7\text{F}_1$ are called magnetic dipole transitions, and the transitions of $^5\text{D}_0$ to $^7\text{F}_{0,2,3,4}$ are called electric dipole transitions. In the case of Eu^{3+} , the electric dipole transition from the excited state $^5\text{D}_0$ to the

${}^7F_{0,2,3,4}$ level is forbidden if the substitution site has an inversion symmetry. On the other hand, it is known that the occurrence probability of a magnetic dipole transition is irrelevant to symmetry. When an atom or crystal is in the molecule, electrons belonging to the atom of interest undergo a Coulomb interaction from the charge in the surrounding ions. The Coulomb potential due to such a surrounding charge is called the crystal field potential. Due to this crystal field potential, the energy levels of atoms that degenerate in the free atom state split. The degeneracy of the $4f_6$ configuration is partly or totally lifted by several perturbations acting on the Eu^{3+} ion; i.e., electron repulsion, spin-orbit coupling, the crystal-field perturbation and eventually the Zeeman effect. The electron repulsion is the electrostatic interaction between the different electrons in the $4f$ shell. The spin-orbit coupling results from the interaction between the spin magnetic moment of the electron and the magnetic field created by the movement of the electron around the nucleus. The crystal-field effect is caused by the interactions between the $4f$ electrons and the electrons of the ligands. The Zeeman effect is the splitting of the energy levels by an external magnetic field.

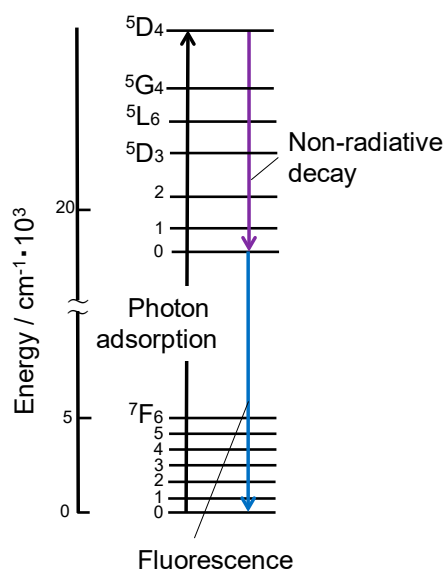


Figure 4. Energy diagram of Eu^{3+} and the possible excitation and decay processes. The excitation processes consist of ${}^7F_0 \rightarrow {}^5D_4$, ${}^7F_0 \rightarrow {}^5G_4$, ${}^7F_0 \rightarrow {}^5L_6$, ${}^7F_0 \rightarrow {}^5D_2$ and ${}^7F_0 \rightarrow {}^5D_1$, and the decay processes corresponded to the transitions from the metastable orbital singlet state of 5D_0 to the spin-orbital states of 7F_J ($J = 0, 1, 2, 3$ and 4) of Eu^{3+} .

The splitting of the terms into the J states by the spin-orbit coupling interaction is on the order of 1000 cm^{-1} . The $2J + 1$ degeneracy of the energy levels in the free ion is further lifted by the crystal-field effect, after which the energy levels are characterized by the irreducible representation of the point group of the Eu^{3+} site [48]. These levels are called crystal-field levels (or Stark levels). The splitting of the energy levels by the crystal-field effect is on the order of a few hundred cm^{-1} or less. In systems with an orthorhombic or lower symmetry, all the degeneracy are lifted by the

crystal field. In systems with a higher symmetry, all of the degeneracy can be lifted by an external magnetic field, via the so-called Zeeman effect. Even in strong magnetic fields, the splitting of the energy levels by the Zeeman effect is only a few cm^{-1} . The J quantum numbers are well defined in the free Eu^{3+} ion, but J -mixing occurs when the Eu^{3+} is located in a non-spherically symmetric ligand environment [49]. J -mixing is induced by the even-parity components of the crystal-field potential.

The energy levels and wave functions of the Eu^{3+} ion can be obtained by diagonalization of the energy matrix [48]. The matrix elements are of the type $\langle \Psi | H | \Psi' \rangle$, where H is the effective-operator Hamiltonian, and Ψ and Ψ' are basis functions of the $4f_n$ configuration ($n = 6$ for Eu^{3+}). The angular parts of the matrix elements can be exactly calculated, whereas the radial parts are treated as adjustable parameters. A parameter set is obtained by optimizing a start set of parameters by a general least-squares fitting process in which the energy differences between the calculated and experimental energy levels are minimized. The total Hamiltonian can be written as the sum of a free-ion and a crystal-field part by the following Equation (2).

$$H = H_{free\ ion} + H_{crystal\ field} \quad (2)$$

The free-ion Hamiltonian is characterized by a set of three electron repulsion parameters (F^2, F^4, F^6), by the spin-orbit coupling constant ζ_{4f} , the Trees configuration interaction parameters (α, β, γ), the three-body configuration interaction parameters ($T^2, T^3, T^4, T^6, T^7, T^8$) and parameters which describe magnetic interactions ($M^0, M^2, M^4, P^2, P^4, P^6$). An additional parameter E_{ave} (ave stands for “average”) takes into account the kinetic energy of the electrons and their interaction with the nucleus. The free-ion Hamiltonian can be written by the following Equation (3) [50,51]:

$$H_{free\ ion} = E_{ave} + \sum_{k=2,4,6} F^k f_k + \zeta_{4f} A_{SO} + \alpha L(L+1) + \beta G(G_2) + \gamma G(R_7) + \sum_{i=2,3,4,6,7,8} T^i t_i + \sum_{j=0,2,4} M^j m_j + \sum_{k=2,4,6} P^k p_k \quad (3)$$

where f_k and A_{SO} represent the angular part of the electrostatic and spin-orbit interaction, respectively. L is the total orbital angular momentum. $G(G_2)$ and $G(R_7)$ are the so-called Casimir operators for the groups G_2 and R_7 , respectively. The t_i are the three-particle operators. The m_j and p_k represent the operators for the magnetic corrections. The F_k parameters decrease if k increases. The terms in the Hamiltonian that represent the non-spherical part of the interactions with the host matrix are described by using the crystal-field Hamiltonian. The crystal-field Hamiltonian can be written by the following Equation (4) [48]:

$$H_{crystal\ field} = \sum_{i=0}^n \sum_{k=0}^{\infty} \sum_{q=-k}^k B_q^k C_q^k(i) \quad (4)$$

where $C_q^k(i)$ are tensor operators of rank k with components q . These tensor operators transform the spherical harmonics. The B_q^k is the

crystal-field parameter, n is the number of electrons (6 in the case of Eu^{3+}) and i represents the i -th electron. The number of non-zero parameters are determined by the point-group site symmetry of the Ln ion. For cell-labeling applications of the Eu^{3+} ions, it is important to change the symmetry and enhance the luminescence.

Table 2. Synthetic temperatures, approximate sizes of primary particles and excitation and luminescence wavelengths of the Eu^{3+} -doped HA in the previous reports [44,54–56].

Synthetic temperature (°C)	Approximate size of primary particle (nm)	Excitation wavelength (nm)	Luminescence wavelength (nm)	Remarks	Reference
Room temperature	9–28	392	612	0.7–1.0 ms (luminescence lifetime)	[44]
40, 120	10–60	393	618	0.7–2.0 ms (luminescence lifetime)	[55]
60	50–200	394	613	-10.6 ± 4.2 mV (zeta potential)	[56]
180	40–190	393	614	2.1 % (internal quantum yield @ excitation wavelength at 393 nm)	[54]

Doping Systems in Hydroxyapatite

There are many ions in vivo that play important roles in the expression of various biological functions. The HA can be given various functions by the substitution of ions in the crystal structure. The studies of ion substitution in the HA crystal structure have been conducted [52–54]. In particular, it is known that the Ca^{2+} can be substituted by various metal ions. **Table 2** shows some reports on the doping of Eu^{3+} ions into the HA structure which is considered to be useful as a cell-label. Among the Ln ions, the Eu^{3+} ion is known to have a low cytotoxicity. The synthesis temperature has been controlled to synthesize the Eu^{3+} ion-doped HA. Excitation and luminescence spectra measurements were performed in the range of the excitation wavelength of 392–394 nm and luminescence wavelength of 612–618 nm [44,54–56]. The internal quantum yield, fluorescence lifetime and zeta potential were reported as other evaluation remarks in the references. The fluorescence lifetime of about 0.7–2.0 ms was achieved [44,55], the zeta potential of about -10.6 mV was reported [56], and the internal quantum yield of 2.1% was achieved by the excitation light irradiation of 394 nm [54]. **Figure 5** shows a diagram of the

coordination structure of oxygen to the Ca site in HA. The Ca (I) site has a coordination number of 9, and C_3 symmetry, and the Ca (II) site has a coordination number of 7, and C_s symmetry. The transition from 5D_0 to 7F_0 is known to indicate the presence of Eu^{3+} ions at the Ca (I) and Ca (II) sites in HA. The 5D_0 to 7F_0 transition peak appears at a maximum fluorescence wavelength of 572 nm at the Ca (I) site and 577 nm at the Ca (II) site [44]. By separating the peak of these two wavelengths, it is possible to evaluate the ratio of Eu^{3+} ions present at the Ca site. The photofunctionalization of HA using the Eu^{3+} ion is the subject of study. However, due to the low internal quantum efficiency, almost no study has been reported on its application in the cell labeling. Thus, the state of Eu^{3+} ions in the HA is important regarding the luminescence behavior.

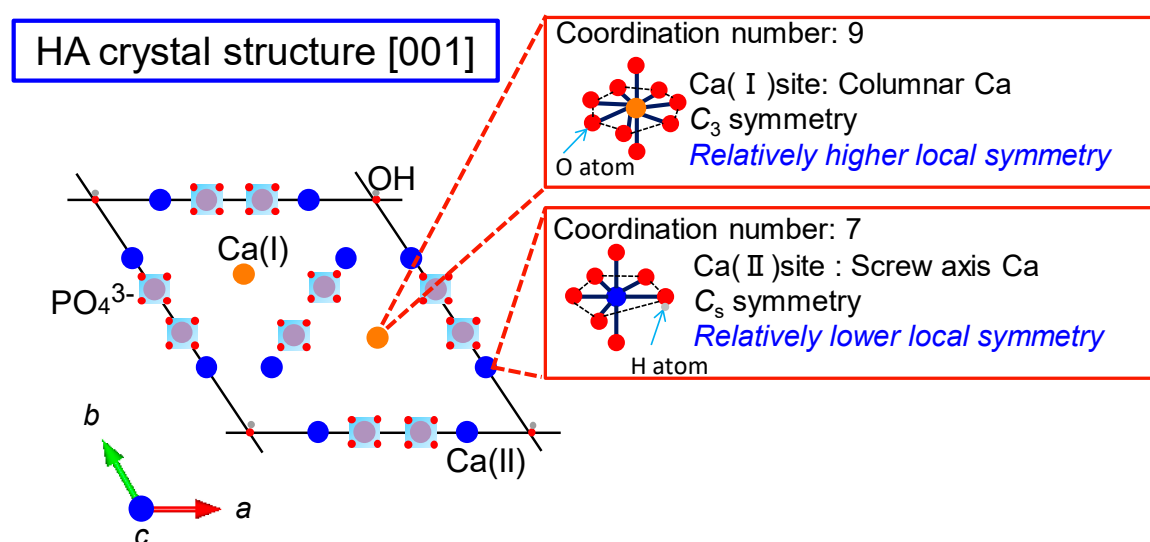


Figure 5. Coordination states of Ca (I) and Ca (II) sites in the HA structure.

Organic Complex Systems

Types and photochemical properties

As functional low molecular weight compounds, the Eu (III) complexes having a ligand are interesting because of their luminescent properties and have been studied in the biofield and the electronics field. The Eu (III) complexes have characteristic narrow luminescence spectrum lines and long-lived excited states. The ligands effectively increase the light absorption. Although the spectral shape depends on the electronic environment, due to the spatially shielded $f-f$ transition, the Eu^{3+} ion alone has a low light absorption ability. It is known that a strong luminescence is observed in the Eu (III) complex in which various ligands are bound to the Eu^{3+} ion. The ligand absorbs the ultraviolet light, and the energy is transferred to the Eu^{3+} ion and finally observed as the luminescence. The effect of ligand is called the antenna effect. When electrons in a singlet ground state molecule are excited to a high energy state by light absorption, they become an excited singlet state (S_1) or an excited triplet state (T_1). The S_1 is a molecular state in which all the electron spins are

paired, and the spins of excited electrons are become the opposite direction to the ground state electrons. In the T_1 , the spins of the excited electrons become the same direction as that of the ground state electrons. Since the excitation to the T_1 includes the inversion of spin, which is a forbidden transition, the probability of the molecule forming the T_1 by light absorption is low. The processes of non-radiatively changing from the S_1 to T_1 or T_1 to S_1 are called intersystem crossing. When the vibrational levels of the two excited states overlap, the probability of intersystem crossing increases because the change in energy due to the transition is low. **Figure 6** shows examples of Eu (III) complexes that have been reported for cell-labeling. Some β -diketonato Eu (III) complexes have been used for the cell-labeling [57,58]. These reports describe that the Eu (III) complex was dissolved in phosphate buffered saline, then cell-labeling was performed. In the case of the β -diketonato Eu (III) complex of **Figure 6a**, the excitation/luminescence spectrum was measured at the excitation wavelength of 402 nm and the luminescence wavelength of 614 nm, and the internal quantum yield was 41% [57]. In the case of the β -diketonato Eu (III) complex of **Figure 6b**, the excitation/luminescence spectrum was measured at the excitation wavelength of 405 nm and the luminescence wavelength of 612 nm, and the internal quantum yield was 23% [58]. However, these available Eu (III) complex luminescent probes have the problem of color degradation, when the probes are exposed to a continuous and intense excitation light for monitoring the biological processes. By introducing an asymmetric coordination field into the Eu (III) complex, the forbidden transition is broken to allow the $f-f$ transition, and the light absorption coefficient can be increased to improve the luminescence intensity. If the symmetry of the ligand can be lowered, application as a cell-labeling probe can be expected.

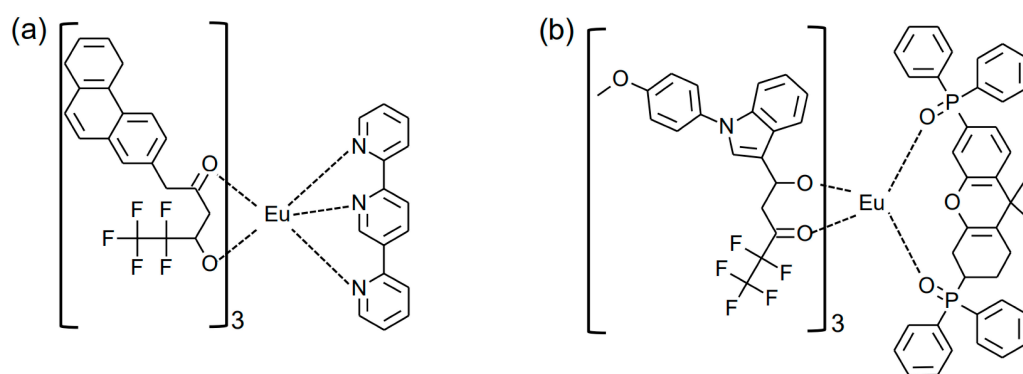


Figure 6. Eu³⁺ complexes of (a, b) β -diketonate ligand [57,58]. Internal quantum yield of (a) is 41% ($\lambda_{\text{ex}} = 402$ nm, $\lambda_{\text{em}} = 614$ nm), and (b) is 23% ($\lambda_{\text{ex}} = 405$ nm, $\lambda_{\text{em}} = 612$ nm). The Eu³⁺ complexes have been studied for biological labelling applications.

Tris(2,2,6,6-tetramethyl-3,5-heptanedionato) europium (III)

The molecular model of *tris(2,2,6,6-tetramethyl-3,5-heptanedionato) europium (III)* (EuTH) as a complex having the diketonato ligand is shown

in **Figure 7**. This complex has a highly-symmetrical molecular structure, and is insoluble in water but soluble in ethanol. Due to the high symmetry of the ligand, the luminescence intensity is low.

In the EuTH, it is known that the distance between the Eu–O and the ligand and the coordination structure affect the electron transition [59]. Different electronic transition states are observed by the coordination symmetry structural change, and the electric dipole transition is strongly observed in the luminescence spectra. Since it can be dissolved in ethanol, the synthesis of a homogeneous hybrid with HA can be expected.

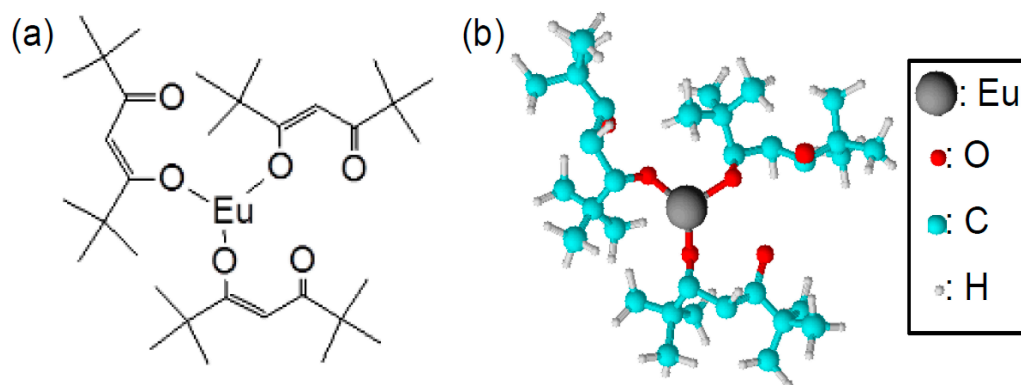


Figure 7. Chemical structures of EuTH molecule at the (a) 2- and (b) 3-dimensional views.

Possibility of hybrid synthesis of hydroxyapatite with EuTH

Ln complexes incorporated into an inorganic porous matrix, such as zeolite or mesoporous silica, that forms an inorganic-organic hybrid have been reported [60,61]. The confinement of the Ln complex within the inorganic porous structure not only improves its stability but also reduces the quenching due to aggregation between the Ln complexes. However, the hybrid with luminescent properties based on the inorganic-organic interface of highly biocompatible HA nanoparticles has not been reported. It is expected that the electron localization between the ligand of the Ln complex and the central metal can be used as a nucleation site of the HA crystals. It was also possible that a high luminescence behavior can be achieved. Specifically, we have been focusing on the electron localization between the central Eu^{3+} ion of EuTH and the diketonate ligand. The nucleation of HA in the electron localization of EuTH resulted in the synthesis of the HA-EuTH hybrid [62,63]. It is suggested that the luminescence intensity can be improved by lowering the symmetry of the EuTH ligand.

SPECIFIC BINDING MOLECULES TO CANCER CELLS

Receptor Expressed on Cell Surface

Receptors are present in all cells. The receptor is a substance and is present on the cell membrane, which specifically binds to a substance outside the cell membrane and is usually a protein. Cells can identify

specific substances by receptors and receive information from outside the cells. Binding of the receptor to the substance triggers a variety of responses in the cell. **Table 3** shows the types of receptors expressed on the surface of epithelial cancer cells that can be treated with an endoscope [64–69].

The types of overexpressed receptors differ depending on the type of cancer. It is known that specific recognition of these receptors enables particle uptake into the cells.

Table 3. Classifications of epithelial cancer cells that can be treated with an endoscope, excess expression receptor on the cells and their binding molecules [64–69].

Classification of cancer	Excess expression receptor	Classification of binding molecule	Reference
Epithelial-derived tumor	α -Folate receptor	α -Folate	[64]
Breast cancer	Estrogen receptor	Estrogen	[65]
Breast cancer or endometrial cancer	Progesterone receptor	Progesterone	[66]
Gastric cancer, breast cancer, ovarian cancer	HER2 receptor	HER2	[67]
Skin cancer	Insulin receptor	Insulin	[68]
Metastatic tumor and drug resistant tumor	Transferrin receptor	Transferrin	[69]

Types of Molecules that Specifically Bind to Receptors

Table 3 also shows the molecules that recognize and specifically bind to the receptors. The recognition of organic molecules or proteins corresponding to the receptor allows the particle uptake into the cells. In order to be used as the cell-labeling nanoparticles, the molecules should be present in the dispersed state on the particle surfaces. The aggregation of the molecules may make it difficult for the receptor to recognize the molecules. Thus, the efficient uptake of HA nanoparticles into the cells becomes possible by immobilizing the cells binding molecules on the HA surface.

Immobilization Technique of Specific Binding Molecule on Solid Surface

By immobilizing a specific binding molecule on a solid surface, it is possible to impart new properties such as in vivo stability, tissue targeting, cell tropism, etc., to the nanoparticle. In order to maximize the properties of the nanoparticles in vivo, it is necessary to achieve surface immobilization techniques that consider the interaction between the cells

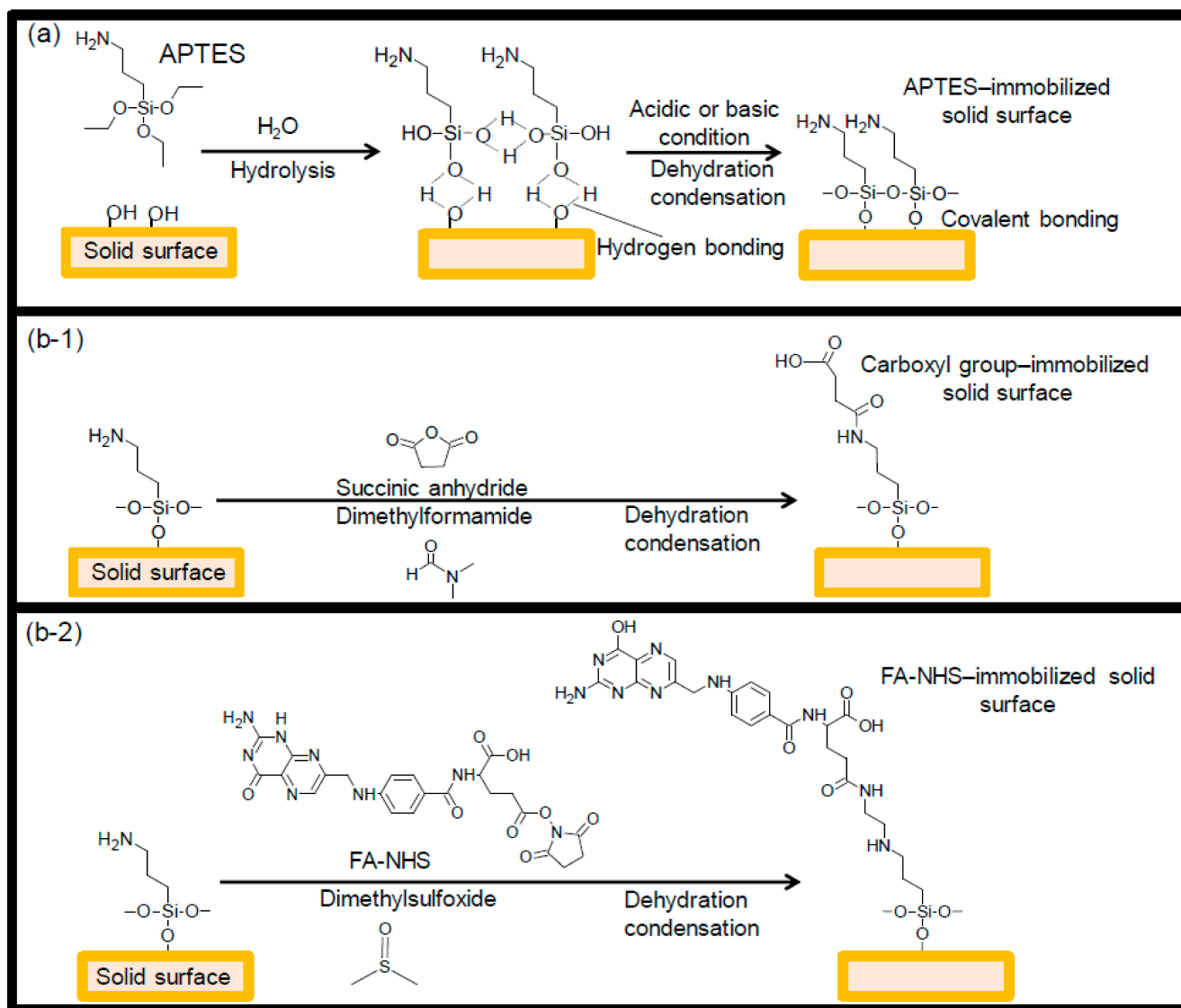


Figure 8. Immobilization processes of (a) APTES, (b-1) carboxyl group and (b-2) FA-NHS on the solid surface. In this case, the representative APTES-immobilized solid surface changed from an amine to (b-1) carboxyl group and (b-2) FA-NHS were shown.

The surface amino group stably immobilizes the molecule through the peptide ($-HN-CO-$) bond. Specifically, APTES is bonded to the solid surface by a liquid phase reaction, the solid surface is coated with the $-Si-O-Si-$ bond, and the amino group is exposed to the surface. Next, the molecule is formed via a covalent bond to the solid surface by a dehydration condensation reaction ($-NH_2 + -COOH \rightarrow -NH-CO-$) of an amino group and a carboxylic acid in the molecule. Such a reaction mechanism makes it possible to immobilize folate derivatives (folate *N*-hydroxysuccinimidyl ester (FA-NHS)), which are known to specifically bind to cancer cells, on the solid surfaces [38]. As the report of the physical surface immobilization technique, the immobilization of ferritin by an electrostatic interaction was achieved on the solid surface [72]. The uptake of the ferritin-immobilized particles into cells was also observed. Thus, for the solid surface, various surface states can be designed.

CANCER CELL GROWTH INHIBITION DRUGS

Representative Molecules and Their Functions

Table 4 shows examples of cytostatic drug molecules. Vitamin C exerts a strong antioxidant action and generates a large amount of hydrogen peroxide [73]. Although normal cells can neutralize hydrogen peroxide, cancer cells cannot neutralize it, causing cell death. Fucoidan has been shown in basic studies to have the function of transmitting stress signals to the endoplasmic reticulum and inducing cell death [74]. Caffeine has been reported to inhibit cancer cell DNA repair and suppress the growth of cancer cells. It has also been reported that the caspase 9/3 pathway, which is one of the signal transduction pathways causing cell death, functions as a persistent anticancer agent by activation [75]. Citric acid is known to induce cell death by inhibiting the function of proteins involved in cell growth by forming a chelate in the cell with minerals such as iron and calcium [76,77]. It has also been reported that the glycolytic system of the cell is inhibited to suppress proliferation [78]. If these drug molecules can be hybridized with the HA, they may be applied as the nanoparticles for cancer therapy.

Table 4. Mechanism and function of cytostatic drug molecules in the previous reports [73–78].

Cytostatic drug molecules	Mechanism	Function	Reference
Vitamin C	Damage of tumor cell due to high dosage	Damage of tumor cells by generation of hydrogen peroxide	[73]
Fucoidan	Induction of apoptosis of cancer cells	Anti-tumor function by modulating endoplasmic reticulum stress cascades	[74]
Caffeine	Induction of apoptosis by activating the caspase-9/-3 pathway	Function as a sustained anticancer agent by activating the caspase-9/-3 pathway	[75]
Citric acid	Suppression of tumor cell growth both in glycolysis and tricarboxylic acid cycles in vitro	Suppression of lung cancer cell growth by dosage	[76–78]

Citric Acid

Figure 9 shows the molecular structure of citric acid (**Figure 9a**), dissociation state in solution (**Figure 9b**) and mechanism of suppression of cancer cell growth by citric acid in the cancer cells (**Figure 9c**). When the amount of citric acid is increased in the cancer cells, chelates are formed with calcium, iron, copper and zinc, which inhibit the action of proteins and antioxidant enzymes involved in cell growth. As a result, it

has been reported to suppress the growth of cancer cells and induce cell death. In the blood, iron (III) ions (Fe^{3+}) bind to transferrin and are transported into the cells. Two Fe^{3+} ions bind to one transferrin. Transferrin binds to the transferrin receptor located on the cell membrane and is taken up by endocytosis. When it becomes an acidic environment in the lysosome (endosome), Fe^{3+} ions are then dissociated into iron (II) ions (Fe^{2+}). It then forms the chelate complex with citric acid, depletes Fe^{2+} ions in the cytoplasm, and inhibits the growth of the cells [79]. The dissociation constant pK_{Fe} between citric acid and Fe^{2+} ion is about 19.7 [80], and the dissociation constant pK_{Ca} between citric acid and Ca^{2+} ion is about 4.3 [81]. In the cells, stable chelates are formed between the Fe^{2+} ions and citric acid. In normal cells (e.g., prostatic epithelium cells) [82], it is known that the addition of citric acid has no effect on the cellular activity.

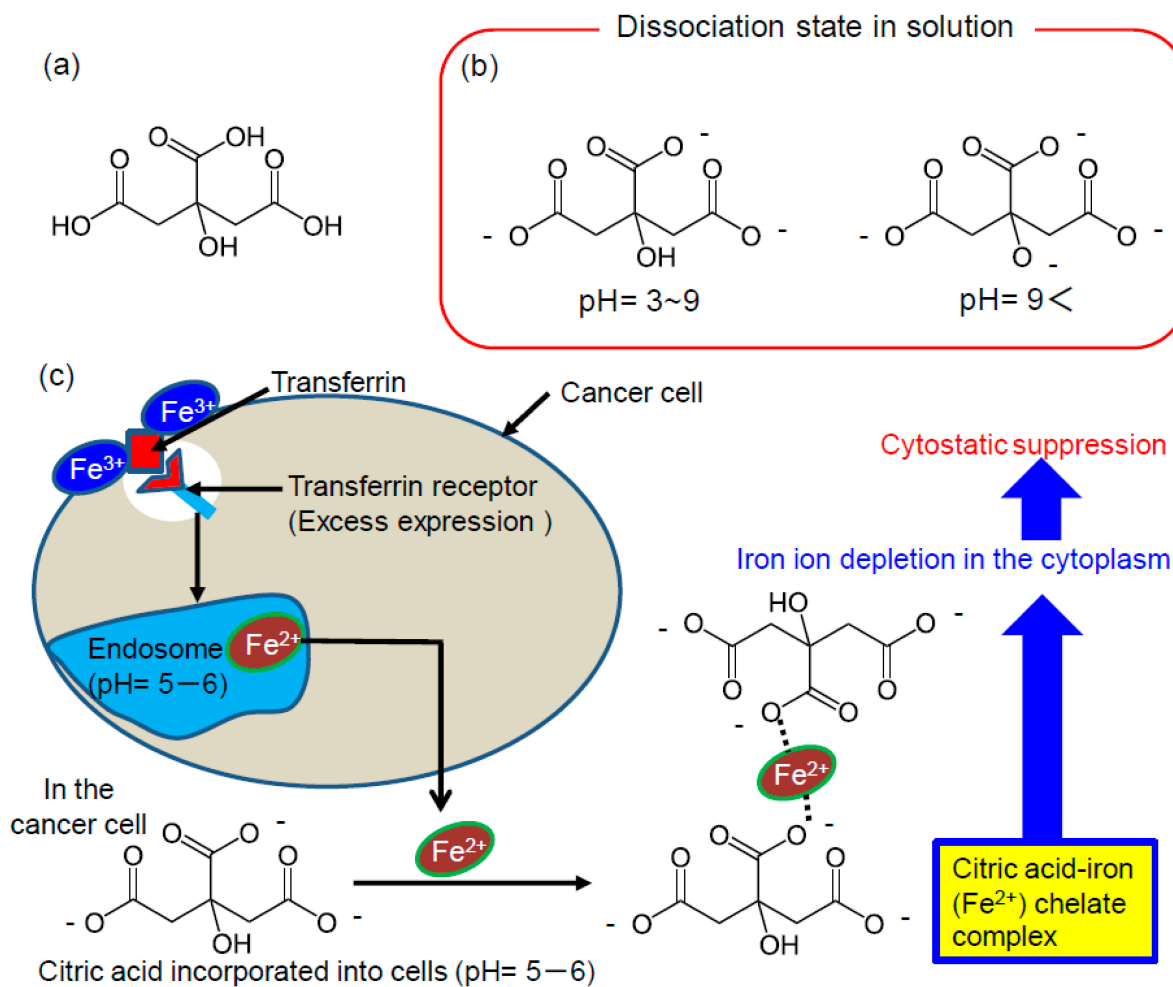


Figure 9. (a) Chemical structure of citric acid and (b) dissociated state in solution at the different pH ($\text{pK}_{\text{a}1} = 3.12$, $\text{pK}_{\text{a}2} = 4.76$, $\text{pK}_{\text{a}3} = 6.39$). (c) Cytostatic mechanism by citric acid. Citric acid and Fe^{2+} ions can form a chelate complex, and the depletion of Fe^{2+} ions in the cytoplasm can suppress the cancer cell proliferation. The dissociation constant pK_{Fe} between citric acid and iron (II) is about 19.7, and the dissociation constant pK_{Ca} between citric acid and Ca^{2+} is about 4.3. In the cells, stable chelates are formed between Fe^{2+} and citrate.

Hydroxyapatite Nanoparticles Functionalized with Citric Acid Molecules

Citric acid molecule is used to control the form of HA and is known to exist as the carboxyl ion of -COO^- in alkaline solution and as a dimer by hydrogen bonding in the form of $(\text{-COOH})_2$ in an acidic solution [83]. Since HA has Ca sites in the *a*-axis direction and phosphate sites in the *c*-axis direction, it has been thought that citric acid molecule adsorbs on the Ca sites and affects the formation of the HA nanoparticles. During HA formation in alkaline solution, it has been suggested that the carboxyl ion of the citric acid molecule and Ca^{2+} ions of HA chemically bond perpendicular to *a*-plane (100) on the HA. Citric acid molecule easily forms the chelate with the Ca^{2+} ions of the HA. On the basis of these results, it has been considered that the competitive reaction between the HA formation and chelate formation enables the synthesis of hybrid nanoparticles. The synthesis of hybrid nanoparticles can be achieved by utilizing the interaction between ions present at the Ca sites in the HA and carboxyl ions of citric acid molecule.

CONCLUSIONS AND FUTURE PERSPECTIVES

Various types of cell-labeling nanomaterials that stain specific cells have been developed for the non-cytotoxicity visualization. However, two significant problems are known such as color degradation and toxicity in conventional nanomaterials. HA is one of the excellent options to overcome the barriers based on its high biocompatibility; HA is present as a main component of hard tissues in vivo, making it possible to be utilized as a biomaterial. When aiming at the cell-labeling application of HA, it is important to bind a photofunctional molecule with HA in the nucleation process and to synthesize nanoparticles as a form of inorganic-organic hybrid. We have achieved rapid cell-labeling through specific uptake into cancer cells and an easily observable luminescence using the HA-organic complex hybrid. Further studies are now in progress to develop theranostic nanoparticles with fluorescence and therapeutic properties toward future applications in such a field as biomedicine. In order to design novel theranostic nanomaterials, one of the keys would be to control interfacial interactions between HA and organic molecules. To explore the combination of HA and various organic molecules will lead to a large number of multifunctional nanoparticles that advance the frontier technologies of bio-related fields.

CONFLICTS OF INTEREST

The authors declare that they have no conflicts of interest.

FUNDING

This review paper was supported by a grant from the Japan Society for the Promotion of Science (JSPS) KAKENHI (Grant-in-Aid for Young

Scientists (A), Grant No. 17H04954, and Grant-in-Aid for JSPS Fellows, Grant No. 18J20271).

REFERENCES

1. Zhang M, Yu M, Li F, Zhu M, Li M, Gao Y, et al. A highly selective fluorescence turn-on sensor for cysteine/homocysteine and its application in bioimaging. *J Am Chem Soc.* 2007;129:10322-3.
2. Zhu S, Meng Q, Wang L, Zhang J, Song Y, Jin H, et al. Highly photoluminescent carbon dots for multicolor patterning, sensors, and bioimaging. *Angew Chem.* 2013;125:4045-9.
3. Yang Y, Zhao Q, Feng W, Li F. Luminescent chemodosimeters for bioimaging. *Chem Rev.* 2013;113:192-270.
4. Ray SC, Saha A, Jana NR, Sarkar R. Fluorescent carbon nanoparticles: Synthesis, characterization, and bioimaging application. *J Phys Chem C.* 2009;113:18546-51.
5. Müller C, Zhernosekov K, Köster U, Johnston K, Dorrer H, Hohn A, et al. A unique matched quadruplet of terbium radioisotopes for PET and SPECT and for α - and β -radionuclide therapy: An in vivo proof-of-concept study with a new receptor-targeted folate derivative. *J Nucl Med.* 2012;53:1951-9.
6. Hadjipanayis CG, Bonder MJ, Balakrishnan S, Wang X, Mao H, Hadjipanayis GC. Metallic iron nanoparticles for MRI contrast enhancement and local hyperthermia. *Small.* 2008;4:1925-9.
7. Achilefu S. Lighting up tumors with receptor-specific optical molecular probes. *Technol Cancer Res Treat.* 2004;3:393-409.
8. Noriya U, Ryu I, Hiroyasu I. Diagnosis of upper gastrointestinal diseases using autofluorescence imaging videoendoscopy system. *Nippon Laser Igakkaishi.* 2009;30:37-40.
9. Masuda S, Yanase Y, Usukura E, Ryuzaki S, Wang P, Okamoto K, et al. High-resolution imaging of a cell-attached nanointerface using a gold-nanoparticle two-dimensional sheet. *Sci Rep.* 2017;7:1-10.
10. Zaki NM, Tirelli N. Gateways for the intracellular access of nanocarriers: A review of receptor-mediated endocytosis mechanisms and of strategies in receptor targeting. *Expert Opin Drug Deliv.* 2010;7:895-913.
11. Roth TF, Porter KR. Yolk protein uptake in the oocyte of the mosquito *Aedes aegypti*. *J Cell Biol.* 1964;20:313-32.
12. Monier S, Parton RG, Vogel F, Behlke J, Henske A, Kurzchalia TV. VIP21-caveolin, a membrane protein constituent of the caveolar coat, oligomerizes in vivo and in vitro. *Mol Biol Cell.* 1995;6:911-27.
13. Kumari A, Sharma A, Malairaman U, Singh RR. Proficient surface modification of CdSe quantum dots for highly luminescent and biocompatible probes for bioimaging: A comparative experimental investigation. *J Lumin.* 2018;199:174-82.
14. Wang L, Li W, Li M, Su Q, Li Z, Pan D, et al. Ultrastable amine, sulfo cofunctionalized graphene quantum dots with high two-photon fluorescence for cellular imaging. *ACS Sustain Chem Eng.* 2018;6:4711-6.

15. Li Z, Miao H, Fu Y, Liu Y, Zhang R, Tang B. Fabrication of NaYF₄:Yb,Er Nanoprobes for Cell Imaging Directly by Using the Method of Hydrion Rivalry Aided by Ultrasonic. *Nanoscale Res Lett.* 2016;11:1-10.
16. Escudero A, Carrillo-Carrión C, Zyuzin MV, Ashraf S, Hartmann R, Núñez NO, et al. Synthesis and functionalization of monodisperse near-ultraviolet and visible excitable multifunctional Eu³⁺, Bi³⁺:REVO₄ nanophosphors for bioimaging and biosensing applications. *Nanoscale.* 2016;8:12221-36.
17. Miyawaki A, Niino Y. Molecular Spies for Bioimaging-Fluorescent Protein-Based Probes. *Mol Cell.* 2015;58:632-43.
18. Chan J, Dodani SC, Chang CJ. Reaction-based small-molecule fluorescent probes for chemoselective bioimaging. *Nat Chem.* 2012;4:973-84.
19. Okabe K, Inada N, Gota C, Harada Y, Funatsu T, Uchiyama S. Intracellular temperature mapping with a fluorescent polymeric thermometer and fluorescence lifetime imaging microscopy. *Nat Commun.* 2012;3:1-9.
20. Fukazawa A, Suda S, Taki M, Yamaguchi E, Grzybowski M, Sato Y, et al. Phospha-fluorescein: a red-emissive fluorescein analogue with high photobleaching resistance. *Chem Commun.* 2016;52:1120-3.
21. Shen J, Zhu Y, Yang X, Li C. Graphene quantum dots: emergent nanolights for bioimaging, sensors, catalysis and photovoltaic devices. *Chem Commun (Camb).* 2012;48:3686-99.
22. Zako T, Nagata H, Terada N, Sakono M, Soga K, Maeda M. Improvement of dispersion stability and characterization of upconversion nanophosphors covalently modified with PEG as a fluorescence bioimaging probe. *J Mater Sci.* 2008;43:5325-30.
23. Wang H, Uehara M, Nakamura H, Miyazaki M, Maeda H. Synthesis of well-dispersed Y₂O₃:Eu nanocrystals and self-assembled nanodisks using a simple non-hydrolytic route. *Adv Mater.* 2005;17:2506-9.
24. Koutsopoulos S. Synthesis and characterization of hydroxyapatite crystals: A review study on the analytical methods. *J Biomed Mater Res.* 2002;62:600-12.
25. Fabiola V, Salvador M, Claudia OM, Julio MA, Juan LA. Antibody-coupled hydroxyapatite nanoparticles as efficient tools for labeling intracellular proteins. *Mater Sci Eng C.* 2017;71:909-18.
26. Vines JB, Lim DJ, Anderson JM, Jun HW. Hydroxyapatite nanoparticle reinforced peptide amphiphile nanomatrix enhances the osteogenic differentiation of mesenchymal stem cells by compositional ratios. *Acta Biomater.* 2012;8:4053-63.
27. Shi Z, Huang X, Cai Y, Tang R, Yang D. Size effect of hydroxyapatite nanoparticles on proliferation and apoptosis of osteoblast-like cells. *Acta Biomater.* 2009;5:338-45.
28. Kirschvink JL, Lowenstam HA. Mineralization and magnetization of chiton teeth: paleomagnetic, sedimentologic, and biologic implications of organic magnetite. *Earth Planet Sci Lett.* 1979;44:193-204.
29. Brooker LR, Lee AP, Macey DJ, Van Bronswijk W, Webb J. Multiple-front iron-mineralisation in chiton teeth (*Acanthopleura echinata*: Mollusca: Polyplacophora). *Mar Biol.* 2003;142:447-54.

30. Gordon LM, Joester D. Nanoscale chemical tomography of buried organic-inorganic interfaces in the chiton tooth. *Nature*. 2011;469:194-8.
31. Kim S, Park CB. Bio-inspired synthesis of minerals for energy, environment, and medicinal applications. *Adv Funct Mater*. 2013;23:10-25.
32. Mikami Y, Tsuda H, Akiyama Y, Honda M, Shimizu N, Suzuki N, et al. Alkaline phosphatase determines polyphosphate-induced mineralization in a cell-type independent manner. *J Bone Miner Metab*. 2016;34:627-37.
33. Simons B. Passive transport and binding of lead by human red blood cells. *J Physiol*. 1986;378:267-86.
34. Skou JC. Enzymatic basis for active transport of Na⁺ and K⁺ across cell membrane. *Physiol Rev*. 1965;45:596-617.
35. Deshmukh K, Shaik MM, Ramanan SR, Kowshik M. Self-activated fluorescent hydroxyapatite nanoparticles: a promising agent for bioimaging and biolabeling. *ACS Biomater Sci Eng*. 2016;28:1257-64.
36. Guang J, Haifang W, Lei Y, Xiang W, Rongjuan P, Tao Y, et al. Cytotoxicity of carbon nanomaterials: single-wall nanotube, multi-wall nanotube, and fullerene. *Environ Sci Technol*. 2005;39:1378-83.
37. International Organization for Standardization (ISO). Biological evaluation of medical devices Part 5: Tests for in vitro cytotoxicity. Geneva (CH): ISO; 2009. ISO 10993-5:2009.
38. Kataoka T, Abe S, Tagaya M. Surface-engineered design of efficient luminescent europium(III) complex-based hydroxyapatite nanocrystals for rapid HeLa cancer cell imaging. *ACS Appl Mater Interfaces*. 2019;11:8915-27.
39. Matsuya T, Otsuka Y, Tagaya M, Motozuka S, Ohnuma K, Mutoh Y. Formation of stacked luminescent complex of 8-hydroxyquinoline molecules on hydroxyapatite coating by using cold isostatic pressing. *Mater Sci Eng C*. 2016;58:127-32.
40. Tagaya M, Motozuka S. An investigation into photofunctional interfaces of 8-hydroxyquinoline/hydroxyapatite hybrids. *Opt Mater*. 2017;66:392-8.
41. Luo H, Li W, Ji D, Zuo G, Xiong G, Zhu Y, et al. One-step exfoliation and surface modification of lamellar hydroxyapatite by intercalation of glucosamine. *Mater Chem Phys*. 2016;173:262-7.
42. Ming M, Wei-Peng L, Xiao-Feng C, Ke-Ya M, Yan-Chuan G. Luminescent and cytotoxic characteristics of an ellipsoidal and micro-sized europium (Eu)-doped hydroxyapatite. *J Inorg Mater*. 2016;31:890-6.
43. Han Y, Wang X, Dai H, Li S. Synthesis and luminescence of Eu³⁺ doped hydroxyapatite nanocrystallines: Effects of calcinations and Eu³⁺ content. *J Lumin*. 2013;135:281-7.
44. Kataoka T, Shiba K, Tagaya M. Preparation of europium(III)-doped hydroxyapatite nanocrystals in the presence of cationic surfactant. *Colloids Interface Sci Commun*. 2016;13:1-5.
45. Kouyate D, Ronfard-Haret J-C, Kossanyi J. Photo- and electro-luminescence of rare earth-doped semiconducting zinc oxide electrodes: Emission from both the dopant and the support. *J Lumin*. 1991;50:205-10.
46. Binnemans K. Interpretation of europium(III) spectra. *Coord Chem Rev*. 2015;295:1-45.

47. Freeman AJ, Watson RE. Theoretical investigation of some magnetic and spectroscopic properties of rare-earth ions. *Phys Rev.* 1962;127:2058-75.
48. Görller-Walrand C, Binnemans K. Chapter 155 Rationalization of crystal-field parametrization. *Handb Phys Chem Rare Earths.* 1996;23:121-283.
49. Berry MT, Reid MF, Richardson FS. The ligand dependence of lanthanide $4f \rightarrow 4f$ magnetic dipole transition moments. *J Chem Phys.* 1986;84:2917-25.
50. Crosswhite HM, Crosswhite H. Parametric model for f -shell configurations. I. The effective-operator Hamiltonian. *J Opt Soc Am B.* 1984;1:246-54.
51. Carnall WT, Goodman GL, Rajnak K, Rana RS. A systematic analysis of the spectra of the lanthanides doped into single crystal LaF_3 . *J Chem Phys.* 1989;90:3443-57.
52. Lin K, Liu P, Wei L, Zou Z, Zhang W, Qian Y, et al. Strontium substituted hydroxyapatite porous microspheres: Surfactant-free hydrothermal synthesis, enhanced biological response and sustained drug release. *Chem Eng J.* 2013;222:49-59.
53. Yuan Q, Wu J, Qin C, Xu A, Zhang Z, Lin S, et al. Spin-coating synthesis and characterization of Zn-doped hydroxyapatite/polylactic acid composite coatings. *Surf Coatings Technol.* 2016;307:461-9.
54. Escudero A, Calvo ME, Rivera-Fernández S, de la Fuente JM, Ocaña M. Microwave-assisted synthesis of biocompatible europium-doped calcium hydroxyapatite and fluoroapatite luminescent nanospindles functionalized with poly(acrylic acid). *Langmuir.* 2013;29:1985-94.
55. Al-Kattan A, Dufour P, Dexpert-Ghys J, Drouet C. Preparation and physicochemical characteristics of luminescent apatite-based colloids. *J Phys Chem C.* 2010;114:2918-24.
56. Yan-Zhong Z, Yan-Yan H, Jun Z, Shai-Hong Z, Zhi-You L, Ke-Chao Z. Characteristics of functionalized nano-hydroxyapatite and internalization by human epithelial cell. *Nanoscale Res Lett.* 2011;6:1-8.
57. Divya V, Sankar V, Raghu KG, Reddy MLP. A mitochondria-specific visible-light sensitized europium β -diketonate complex with red emission. *Dalt Trans.* 2013;42:12317-23.
58. George TM, Krishna MS, Reddy MLP. A lysosome targetable luminescent bioprobe based on a europium β -diketonate complex for cellular imaging applications. *Dalt Trans.* 2016;45:18719-29.
59. Nelson BN, Caster AG, Berry MT. Gas-phase photoionization of tris(2,2,6,6-tetramethyl-3,5-heptanedionato) europium(III). *Chem Phys Lett.* 2004;396:256-60.
60. Yan B, Zhou B. Two photoactive lanthanide (Eu^{3+} , Tb^{3+}) hybrid materials of modified β -diketone bridge directly covalently bonded mesoporous host (MCM-41). *J Photochem Photobiol A Chem.* 2008;195:314-22.
61. Li P, Wang Y, Li H, Calzaferri G. Luminescence enhancement after adding stoppers to europium(III) nanozeolite L. *Angew Chem.* 2014;53:2904-9.
62. Kataoka T, Shinozaki K, Abe S, Tagaya M. Preparation of calcium phosphate nanoparticles hybridized with europium (III) complex for novel luminescent organic-inorganic systems. *J Phys Chem Solids.* 2018;122:218-26.

63. Kataoka T, Shiba K, Tagaya M. An investigation into nanohybrid states of europium (III) complex with hydroxyapatite nanocrystals. *Opt Mater.* 2018;84:252-8.
64. Hilgenbrink AR, Low PS. Folate Receptor-Mediated Drug Targeting: From Therapeutics to Diagnostics. *J Pharm Sci.* 2005;94:2135-46.
65. Brzozowski AM, Pike ACW, Dauter Z, Hubbard RE, Bonn T, Engström O, et al. Molecular basis of agonism and antagonism in the oestrogen receptor. *Nature.* 1997;389:753-8.
66. Horwitz K, McGuire W. Estrogen control of progesterone receptor in human breast cancer: correlation with nuclear processing of estrogen receptor. *J Biol Chem.* 1978;253:2223-8.
67. Scaltriti M, Rojo F, Ocana A, Anido J, Guzman M, Cortes J, et al. Expression of p95HER2, a truncated form of the HER2 receptor, and response to anti-HER2 therapies in breast cancer. *J Natl Cancer Inst.* 2007;99:628-38.
68. Hotamisligil GS, Peraldi P, Budavari A, Ellis R, White MF, Spiegelman BM. IRS-1-mediated inhibition of insulin receptor tyrosine kinase activity in TNF- α - and Obesity-induced insulin resistance. *Science.* 1996;271:665-8.
69. Huebers HA, Beguin Y, Pootrakul P, Einspahr D, Finch CA, Sasaki K, et al. Intact transferrin receptors in human plasma and their relation to erythropoiesis. *Blood.* 1990;75:102-7.
70. Olariu CI, Yiu HHP, Bouffier L, Nedjadi T, Costello E, Williams SR, et al. Multifunctional Fe₃O₄ nanoparticles for targeted bi-modal imaging of pancreatic cancer. *J Mater Chem.* 2011;21:12650-9.
71. Lebret V, Raehm L, Durand J-O, Smaïhi M, Werts MHV, Blanchard-Desce M, et al. Folic acid-targeted mesoporous silica nanoparticles for two-photon fluorescence. *J Biomed Nanotechnol.* 2010;6:176-80.
72. Yamada K, Yoshii S, Kumagai S, Fujiwara I, Nishio K, Okuda M, et al. High-density and highly surface selective adsorption of protein-nanoparticle complexes by controlling electrostatic interaction. *Jpn J Appl Phys.* 2006;45:4259-64.
73. Doskey CM, Buranasudja V, Wagner BA, Wilkes JG, Du J, Cullen JJ, et al. Tumor cells have decreased ability to metabolize H₂O₂: Implications for pharmacological ascorbate in cancer therapy. *Redox Biol.* 2016;10:274-84.
74. Chen S, Zhao Y, Zhang Y, Zhang D. Fucoidan induces cancer cell apoptosis by modulating the endoplasmic reticulum stress cascades. *PLoS One.* 2014;9:1-10.
75. Liu H, Zhou Y, Tang L. Caffeine induces sustained apoptosis of human gastric cancer cells by activating the caspase-9/caspase-3 signalling pathway. *Mol Med Rep.* 2017;16:2445-54.
76. Johnson S. Do mitochondria regulate cellular iron homeostasis through citric acid and haem production? Implications for cancer and other diseases. *Med Hypotheses.* 2003;60:106-11.
77. Kozłowski H, Janicka-Kłos A, Brasun J, Gaggelli E, Valensin D, Valensin G. Copper, iron, and zinc ions homeostasis and their role in neurodegenerative disorders (metal uptake, transport, distribution and regulation). *Coord Chem Rev.* 2009;253:2665-85.

78. Ren JG, Seth P, Ye H, Guo K, Hanai JI, Husain Z, et al. Citrate suppresses tumor growth in multiple models through inhibition of glycolysis, the tricarboxylic acid cycle and the IGF-1R pathway. *Sci Rep.* 2017;7:1-13.
79. Hann HW, Stahlhut MW, Hann CL. Effect of iron and desferoxamine on cell growth and in vitro ferritin synthesis in human hepatoma cell lines. *Hepatology.* 1990;11:566-9.
80. Pierre JL, Gautier-Luneau I. Iron and citric acid: A fuzzy chemistry of ubiquitous biological relevance. *BioMetals.* 2000;13:91-6.
81. De Robertis A, Gianguzza A, Sammartano S. Solubility of some calcium-carboxylic ligand complexes aqueous solution. *Talanta.* 1995;42:1651-62.
82. Mycielska ME, Patel A, Rizaner N, Mazurek MP, Keun H, Patel A, et al. Citrate transport and metabolism in mammalian cells: Prostate epithelial cells and prostate cancer. *BioEssays.* 2009;31:10-20.
83. Toyama T, Oshima A, Yasue T. Hydrothermal synthesis of hydroxyapatite whisker from amorphous calcium phosphate and the effect of carboxylic acid. *J Ceram Soc Japan.* 2011;109:232-7.

How to cite this article:

Kataoka T, Shiba K, Tagaya M. Design of Hydroxyapatite-Based Multifunctional Nanoparticles for Cell Labelling and Cell Growth Inhibition. *Regen Med Front.* 2020;2(1):e200001. <https://doi.org/10.20900/rmf20200001>